Using SeaWiFS Measurements to evaluate Long-term Radiometric Stability of Pseudo-invariant Calibration Sites

Chi Li, Yong Xue[1], *Senior Member, IEEE*, Quanhua Liu, Karim Ouazzane, and Jiahua Zhang

***Abstract*—Pseudo-invariant calibration sites (PICSs) have been widely applied to satellite sensor radiometric calibrations and inter-comparisons. However, the stability of those sites is rarely evaluated comprehensively. We adopted the lifetime Sea-Viewing Wide Field-of-View Sensor (SeaWiFS) radiance data from 1997 to 2010 to monitor the stability of the SeaWiFS reflectance at the top of atmosphere (TOA) over six CEOS (the Committee on Earth Observation Satellites) reference standard PICSs. Cloud-free and spatially homogeneous time series of the mean spectral TOA reflectance (ρ_{TOA}) at eight SeaWiFS channels over these sites are generated together with corresponding observing geometries. We then fit the derived SeaWiFS ρ^{TOA} time series to the Ross-Li Bidirectional reflectance distribution functions (BRDF) model after screening out outliers to characterize the directional reflectivity effects. Time Series of BRDF-normalized spectral TOA reflectance (R^{TOA}) is presented and quantitatively analyzed afterwards. Overall good stability during the SeaWiFS operation period is exhibited, while both root mean square (RMS) and trend slope analysis reveal spectral dependence of the PICSs' stability, i.e. the uncertainty and changing extent of R^{TOA} appear to be larger at shortwave visible (SV) channels (~3%) compared to that of red/near infrared (NIR) bands (~1.5%). The derived results could be utilized or consulted for various calibration applications such as Advanced Very High Resolution Radiometer (AVHRR) recalibration.**

***Index Terms*—pseudo-invariant sites (PICSs), radiometric calibration, SeaWiFS, Top of atmosphere (TOA) reflectance, Bidirectional reflectance distribution functions (BRDF) model**

1. INTRODUCTION

IN an era with everlastingly growing number of Earth observation satellites (EOS), more urgent requirements on the EOS data quality and consistency are proposed for the studies of Earth system, atmosphere process and global climate change, and it is crucial to achieve the synergy of multi-platform satellite data record since the orbit lifetime of satellite instruments are relatively short compared with the time scale of climate change [1, 2]. Radiometric calibration of satellite sensors is a critical prerequisite for this purpose [3, 4]. Attributing to their stable surface characteristics and corresponding

[1] Corresponding author

atmospheric profiles, pseudo-invariant calibration sites (PICSs) have been long adopted for sensor stability monitoring and calibration [5, 6], and inter-comparisons [4, 7] to assure accuracy and traceability, and reduce uncertainties of EOS data, especially for the visible/near infrared (VIS/NIR) spectrum. Despite the rapid development of new techniques such as onboard and lunar calibration [8-10], vicarious calibration based on PICSs is still, and will continue to be critical and indispensable for its unique role in calibrating historic data from early satellites without onboard calibration facilities or lunar observations such as the Advanced Very High Resolution Radiometer (AVHRR) [11] or the Enhanced Thematic Mapper (ETM) series [4], and its competitive performance and cost-effectiveness compared with other methods. Therefore much effort has been taken during the past two decades in establishing and employing PICSs around the world. Such progresses are summarized by Cosnefroy *et al.* [12] and Teillet and Chander [1], where the selection criteria of PICSs, such as high spatial homogeneity, low impact from the variations of aerosol and gaseous absorption, flat reflectivity spectrum, weak directional effects etc., were proposed to guarantee long-term radiometric uniformity and stability — the decisive characteristics for calibration applications. Based on these criteria, the Committee on Earth Observation Satellites (CEOS) Working Group on Calibration and Validation (WGCV) identified a set of PICSs (see in Fig. 1) in Africa deserts, while other type of PICSs such as Antarctic ice [13] is also widely found in relative investigations.

However, although promising post-launch absolute/inter calibration results have been reported from a wealth of similar works, the performance of PICS method is largely dependent on the radiometric stability of selected sites, while this

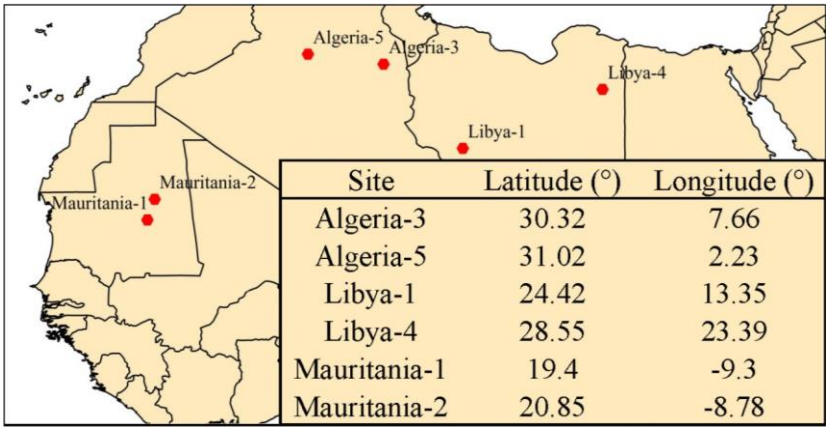

Site	Latitude (°)	Longitude (°)
Algeria-3	30.32	7.66
Algeria-5	31.02	2.23
Libya-1	24.42	13.35
Libya-4	28.55	23.39
Mauritania-1	19.4	-9.3
Mauritania-2	20.85	-8.78

Fig. 1. Distribution of the six CEOS endorsed PICSs.

feature is not comprehensively understood or certificated, especially in terms of long-term quantifications. As the only data resource for long-term statistical analysis, satellite observations have been collected to characterize the temporal behavior of PICSs reflectance in some literatures, whereas most of these studies are confined to a limited span of time (~3 years) and consequently a relatively small amount of data [14], or the quality and stability of employed satellite data as the referenced benchmark is not optimal [12, 15]. Fortunately, innovatively well-calibrated instruments such as the Moderate Resolution Imaging Spectroradiometer (MODIS) and the Sea-viewing Wide Field-of-view Sensor (SeaWiFS)

have collected data for more than a decade and make it possible to conduct long-term stability evaluation of PICSs. Cao *et al.* [13] employed radiance data from MODIS and SeaWiFS to characterize the stability at the red and NIR bands of the DOME C site in the Antarctic, and achieved positive outcomes. Such work should be extended to more sites and spectral ranges in order to complement the characterization of PICSs.

The objective of this study is to quantitatively analyze the long-term stability of the six CEOS endorsed desert PICSs in the whole reflective solar spectrum (0.4 – 1.0 μm) using the lifetime SeaWiFS dataset from 1997 to 2010. In the following section the employed dataset and processing workflow will be outlined. Section 3 provides a comprehensive analysis of derived results, including a quantitative characterization of the revealed trend and stability, and the internal causes are thoroughly discussed, with some consultable suggestions on using these PICSs for calibration purposes. Finally we summarize our study in the last section.

2. Data Processing

SeaWiFS TOA reflectance over PICSs2

From Fig. 1, it is clear that the six PICSs employed for this study, as established by CEOS WGCV subgroup on Infrared Visible Optical Sensors (IVOS), are located in the North African desert. These sites are usually made up of sand dunes with stable atmospheric conditions, which will also be confirmed in later discussions. More details about the PICSs can be found at http://calval.cr.usgs.gov/sites_catalog_ceos_sites.php.

SeaWiFS sensor measures top-of-atmosphere (TOA) solar radiance at eight spectral bands. TABLE I and Fig. 2 present the channel characteristics and relative spectral response (RSR) (http://oceancolor.gsfc.nasa.gov/DOCS/RSR_tables.html). From TABLE I it is found that the Rayleigh optical depth (ROD), NO_2 absorption cross section (k_NO_2), ozone absorption coefficient (k_oz) and absorbing (a_w) and scattering coefficients (b_w) of water vapor differ significantly at each band, revealing the complexity of ocean color remote sensing using multi-spectral information. Nevertheless, after dedicated in-orbit calibration (lunar and solar diffuser measurements) and vicarious technique against the Marine Optical Buoy (MOBY) instrumented site, the SeaWiFS top of atmosphere (TOA) radiance (latest reprocessed in 2010) exhibited an unprecedentedly high level of absolute accuracy, precision and long-term stability throughout the operation time (see [16] for details). Therefore, the time series of SeaWiFS TOA observations over the PICSs would reveal the actual long-term trend and stability characteristics which are determined by changes in the surface reflectivity and perturbations from Rayleigh scattering, aerosols, water vapor and ozone etc. The spatial resolution of local area coverage (LAC) SeaWiFS data is about 1.1 km while 4.5 km for global area coverage (GAC) data. Unfortunately LAC data are only available for limited regions and incomplete periods. To guarantee enough number of cases evenly covering the SeaWiFS lifetime for long-term study, the level 1A GAC data

TABLE I
SEAWIFS CHANNEL CHARACTERISTICS

	Band1	Band2	Band3	Band4	Band5	Band6	Band7	Band8
Wave Center (nm)	413.306	443.944	491.123	510.071	554.631	668.236	764.876	866.353
Wave Width (nm)	20.124	19.608	20.576	22.376	18.293	19.845	40.284	41.366
E_λ ($mW \cdot cm^{-2} \cdot \mu m^{-1}$)	172.998	190.154	196.438	188.164	182.997	151.139	122.33	96.264
ROD	3.13E-01	2.33E-01	1.54E-01	1.33E-01	9.44E-02	4.44E-02	2.55E-02	1.69E-02
k_oz (cm^{-1})	4.11E-04	3.16E-03	2.35E-02	4.09E-02	9.57E-02	4.65E-02	8.14E-03	3.33E-03
k_NO_2 (cm^2)	6.00E-19	4.96E-19	2.75E-19	2.08E-19	9.41E-20	9.23E-21	1.08E-21	1.94E-21
a_w (m^{-1})	4.99E-03	7.51E-03	2.50E-02	4.00E-02	7.71E-02	4.46E-01	2.94E+00	4.87E+00
b_w (m^{-1})	3.27E-03	2.42E-03	1.57E-03	1.34E-03	9.39E-04	4.26E-04	2.38E-04	1.49E-04

ROD stands for Rayleigh optical depth, k_NO_2 is the NO_2 absorption cross section, k_oz means the ozone absorption coefficient, and a_w and b_w each represents the absorbing and scattering coefficients of water vapor (adopted

over the six PICSs are downloaded from the Ocean Color website (http://oceancolor.gsfc.nasa.gov).

Although radiance-based calibration can be found in some papers, the TOA reflectance (ρ^{TOA}) is a widely accepted radiometric quantity eliminating the cosine effect and correcting the variation in the Earth–Sun distance which affects the solar input, especially for multiplatform comparisons and inter-calibration utilities [17]. We generate Level 1B radiance data from L1A products using the SeaWiFS Data Analysis System (SeaDAS) version 6.4 provided by the SeaWiFS Ocean Biology Processing Group (OBPG) data distribution service (available at http://seadas.gsfc.nasa.gov), in which the calibration scheme after the 2010 reprocessing is incorporated. Finally, the calibrated radiance data were converted to ρ^{TOA} according to the following equation:

$$\rho_{\lambda}^{TOA} = \frac{\pi L_\lambda d^2}{E_\lambda \cos\theta_s} \qquad (1)$$

Where L_λ is the sensor received radiance read from the Level 1B data (subscription λ denotes different spectral bands), d stands for the Earth–Sun distance factor, E_λ means the exo-atmospheric solar irradiances at the mean Earth-Sun distance,

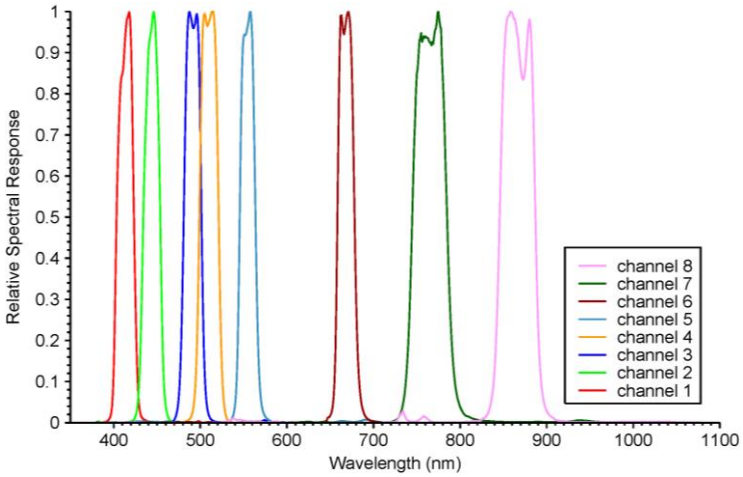

Fig. 2. SeaWiFS channel RSR.

and θ_s represents the solar zenith angle (SZA).

Data Screening

In most studies, the size of area of interest (AOI) is often defined to confine near-nadir observations for reducing directional reflective effects. SeaWiFS is designed to tilt ~20° to avoid sunlight from the sea surface, thus no nadir view is provided, making the bidirectional reflectance distribution functions (BRDF) effects inevitable (we will discuss this later in section 2.3). In this study, pixels in a 3 × 3 window (about 13.5 km wide) centered around the site are taken for every observation, and the mean values of ρ^{TOA} and observing geometry will be stored for further analysis if obeying the following criteria:

1) None of pixels of the window should be contaminated by cloud or next to cloudy pixels. Since SeaWiFS and the MEdium Resolution Imaging Spectrometer (MERIS) have similar spectral channels, we apply the MERIS cloud screening scheme described in [18] to identify cloudy pixels. Considering the lack of thermal infrared bands for comprehensive cloud test, we also reject cloud adjacent pixels, hoping this strict masking will eliminate a large part of cloud effects.
2) Spatial uniformity is tested, and data with a large standard deviation (σ/mean >3% in the window) for any bands are rejected. Residual cloud contamination would also be eliminated through this step since cloud fields are typically inhomogeneous.
3) To reduce outliers caused by abnormal observations, observation noises, and undetected clouds or shadows, the initial time series from the above two steps are updated by removing measurements if window-averaged ρ^{TOA} at any band is above or below 1.5σ from the mean.

The three screening steps synthesize ideas from similar studies [19, 20], and are obviously more stringent, which is favorable for removing instrumental factors to guarantee an effective analysis. In addition, since we have collected 13 year data, the statistical significance of our results will be little affected by the data loss. Fig. 3 shows the case numbers over each PICS after each step. About 50 – 60% cases are screened after the three steps, in which cloud screening corresponds to ~65% of the total data loss. Nevertheless, more than 1000 cases still remain for each site, which stand for the SeaWiFS observation data with high quality, and will be analyzed in detail. More stringent screening criteria could be applied to gain better results if a larger volume of data storage is available [4].

BRDF normalization

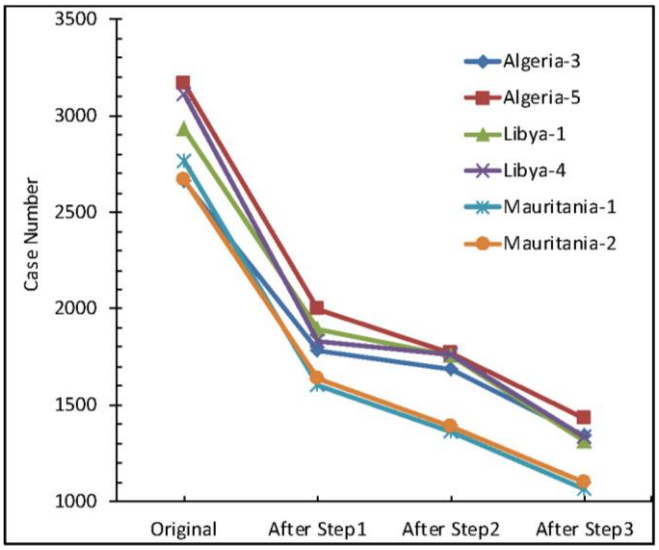

Fig. 3. Number of SeaWiFS observing cases for each site before and after each screening step in section 2.2.

In previous studies employing PICSs, the directional reflective impacts are commonly reduced by confining the observing geometries to a limited range, i.e. near nadir view [4, 20, 21]. However, this strategy would cause a considerable data loss. Moreover, as mentioned above, SeaWiFS provides no nadir view data, and the observing geometries are significantly variable because of sensor tilt and orbit drift [22]. Since the atmospheric effect on ρ^{TOA} is generally recognized as small and stable for the PICSs, their angular distribution could be incorporated into the surface BRDF model to generate a uniform BRDF characterization of ρ^{TOA}, and exhaustive radiative transfer (RT) calculations could be avoided. This idea is adopted in some recent investigations [5, 13]. In this study, the Ross-Thick Li-Sparse BRDF model (employed in the MODIS albedo product [23]) is applied in BRDF fitting of the generated time series of ρ^{TOA}. That means three fixed BRDF parameters are employed to fit the ρ^{TOA} for each PICS and every SeaWiFS band according to Eq. (2).

$$\sum_{i=1}^{n}[\rho_i^{TOA} - \rho(\theta_s,\theta_v,\varphi)]^2 = \min$$
$$\rho(\theta_s,\theta_v,\varphi) = f_{iso} + f_{vol}K_{vol}(\theta_s,\theta_v,\varphi) + f_{geo}K_{geo}(\theta_s,\theta_v,\varphi) \quad (2)$$

Where $\rho(\theta_s, \theta_v, \varphi)$ stands for the BRDF-characterized anisotropic reflectance ρ^{BRDF} at TOA calculated from the BRDF fitting results, n represents the case number of ρ^{TOA} time series after data screening, θ_s, θ_v, φ each means SZA, view zenith angle and relative azimuth angle, respectively. It is noted that subscription λ is omitted while the BRDF fitting parameters (f_{iso}, f_{vol} and f_{geo}, see in TABLE II) are wavelength dependent. In this investigation, the derived BRDF parameters are fitted to the SeaWiFS ρ^{TOA} data in 1997 – 2001 because of potential data quality problem in the last few operational years (we will discuss this in detail in Section 3.3). The fitted BRDF model parameters account for coupled angular effects of surface and atmospheric signals. After obtaining fitted BRDF parameters f_{iso}, f_{vol} and f_{geo} for every PICS at each band, all measurements of the ρ^{TOA} time series are normalized to the BRDF model, as in the formula (3).

$$R^{TOA} = \frac{\rho^{TOA}}{\rho(\theta_s, \theta_v, \varphi)} \quad (3)$$

Theoretically R^{TOA} would be unity if the BRDF fitting is unbiased, i.e. the radiometric stability of evaluated PICS is ideal.

Linear trend analysis

The slope (change per day) and intercept of each linear fitting line for the R^{TOA} time series are calculated based on Chi-square minimization method. The percent change per year of R^{TOA} is simply calculated as the slope multiplied by 365.25. Then the significance of slope is tested with null hypothesis of zero slopes using general T-test method based on formula (4).

$$t = \frac{b\sqrt{\sum_{i=1}^{n}(x_i - \bar{x})^2}}{\sqrt{\frac{1}{n-2}\sum_{i=1}^{n}(y_i - \hat{y}_i)^2}} \sim t(n-2) \quad (4)$$

Where b is the derived slope, x_i and y_i corresponds to the observing time (unit: day) and R^{TOA} each time, $\bar{x}$ means the average of x_i, $\hat{y}_i$ indicates the linear fitted result corresponding to x_i, and n stands for the total observing case number. The p value (doubled probability of greater than the derived $|t|$ value in Eq. (3) for a T-distribution with $n - 2$ degrees of freedom) is generated in each test, and $p < 0.05$ means 95% confidence in rejecting the hull hypothesis (the linear trend is statistically significant). In addition, the Pearson correlation coefficient R is also calculated for each x and y group. Generally larger R value also corresponds to more significance of the derived trend. These linear trending results are summarized in TABLE III.

3. RESULTS AND DISCUSSION

In this section, time series of SeaWiFS measurements over six PICSs are presented and discussed in terms of temporal trend and stability at different channels and sites, while in ahead we will firstly check the BRDF modeling effectiveness which is crucial to draw any conclusions from our investigation.

SeaWiFS Measurements and BRDF modeling

We present the SeaWiFS measured ρ^{TOA} and BRDF modeled ρ^{BRDF} over Algeria-3 as an example in Fig. 4. Due to differences in observing geometries, BRDF effects lead to periodic oscillations (repeating cycle close to one year) in the ρ^{TOA} time series which is discerned in Fig. 4 (a). This annual oscillation is well reproduced by the BRDF model, as the difference between the time series of measurements and model is small. ρ^{TOA} values at shortwave visible (SV) bands (channels 1 – 5) are around 0.17 – 0.28, whereas those at red and NIR bands (channels 6 – 8) are generally larger than

0.38. This signal magnitude difference indicates at the longwave bands the desert surface reflected signal contributes the

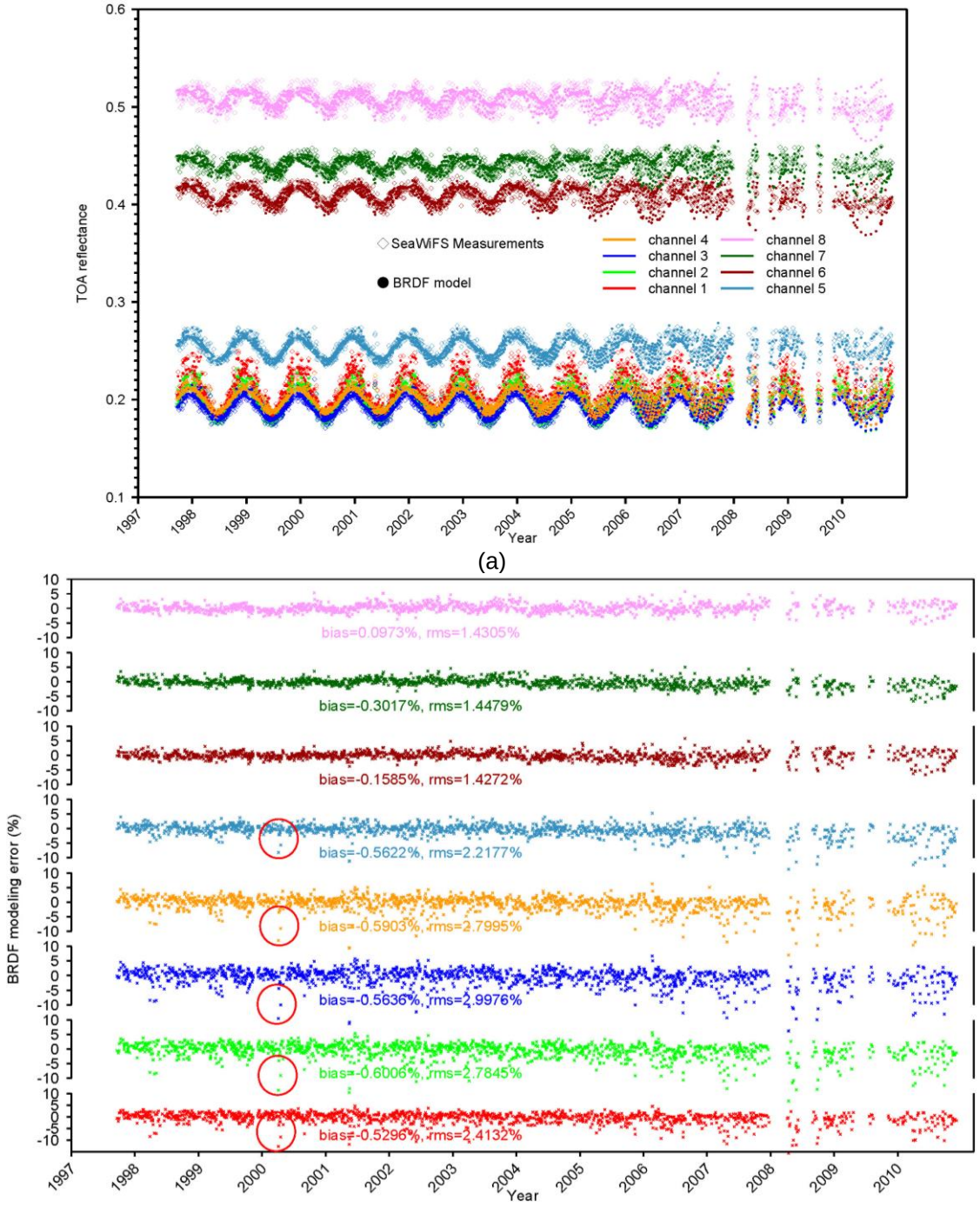

Fig. 4. (a) Time series of TOA reflectance observed by SeaWiFS V.S. BRDF modeling over Algeria-3; (b) Time series of BRDF modeling errors over Algeria-3, red circles indicating exemplified outliers in the plot.

most part in the SeaWiFS measured radiance, while for SV channels atmospheric effects are relatively more significant. There are several data vacuum events since early 2008, mainly due to operation anomalies such as Global Positioning System (GPS) data outage. Since three fixed parameters are adopted in the modeling, the time series of ρ^{BRDF} oscillates periodically in a regular pattern (while measurements scatter moderately around the ρ^{BRDF} points) at the first several years after launch when there are no obvious orbit drift and the passing time of SeaWiFS over each site also varies periodically (Fig. 5). Nevertheless, this regularity of ρ^{BRDF} variation is reduced after 2005, and becomes more and more unpredictable,

indicating that the drift problem is exacerbating. Fig. 5 presents the whole picture of orbit drift over the six PICSs, which are concordant to what we have discovered in the ρ^{BRDF} time series.

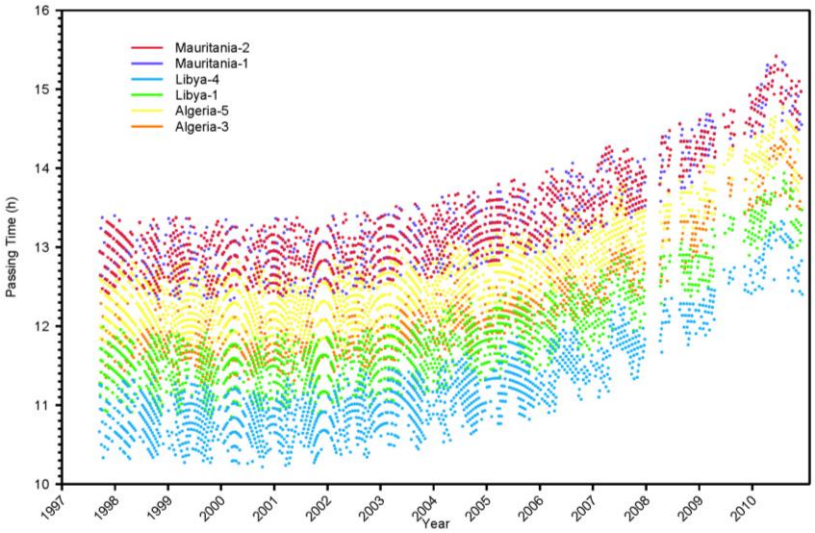

Fig. 5. Time series of SeaWiFS observing time over six PICSs.

The advantage of multi-spectral measurement of SeaWiFS can be revealed from the modeling error scatter diagrams in Fig. 4 (b), where different precision of BRDF modeling in each SeaWiFS channel is obvious. For red/NIR bands, the mean modeling error (bias) is within ~0.3% and the root mean square (RMS) is less than 1.45% despite the orbit drift, confirming that the employed BRDF model is sufficient in characterizing the directional reflectivity feature at these channels. Since at these spectral regions the surface reflectance dominates in the SeaWiFS measured radiance, this modeling precision also indicates little variation of surface directional reflectance characteristics. On the other hand, the BRDF modeling performs inferiorly at SV channels, where observations are more scattered and some outliers could be easily discerned (as in red circles while not found at channels 6 – 8). The bias could reach -0.56% with RMS near 3% at the 491 nm channel. This spectral dependence of BRDF fitting effectiveness is primarily due to the wavelength-dependent atmospheric effects (Rayleigh scattering, aerosol extinction, ozone and water vapor absorption etc.) as seen in TABLE I, since it is not likely to be caused by surface reflectance variation because the surface reflectivity is very stable as revealed by results at channels 6 – 8. Since surface-induced signal is relatively weak, the SV bands are more vulnerably affected by variation of atmospheric effects, e.g. that of aerosols [24], thus resulting in the relatively weak robustness of BRDF fitting at these bands.

The BRDF parameters and the residual errors (bias and RMS) for each band and site are presented in TABLE II. Similar patterns of spectral distribution of BRDF fitting errors (more uncertain at channels 1 – 5) are found for the other the five sites, illustrating the joint characteristics of this kind of desert PICSs. Despite the atmospheric perturbation, a preferable residual within 3% is still achieved at SV bands (~1.5% at red/NIR bands) for most sites except for Mauritania-1/2 (where RMS appears to be systematically larger than other sites at any band), indicating that the atmospheric condition is not drastically variant over these sites, and the BRDF normalized R^{TOA} can reduce a large part of anisotropic effects of ρ^{TOA}

TABLE II
SUMMARY OF BRDF MODELING OVER SIX PICSS

Algeria-3	band1	band2	band3	band4	band5	band6	band7	band8
fiso	0.175	0.172	0.176	0.185	0.239	0.403	0.439	0.504
fvol	0.291	0.234	0.173	0.172	0.188	0.174	0.145	0.164
fgeo	-0.017	-0.012	-0.007	-0.004	0.000	0.010	0.013	0.014
bias (%)	-0.530	-0.601	-0.564	-0.590	-0.562	-0.158	-0.302	0.097
RMS (%)	2.413	2.785	2.998	2.799	2.218	1.427	1.448	1.430
Algeria-5	band1	band2	band3	band4	band5	band6	band7	band8
fiso	0.174	0.171	0.178	0.186	0.236	0.432	0.467	0.545
fvol	0.282	0.223	0.166	0.163	0.180	0.190	0.156	0.176
fgeo	-0.018	-0.013	-0.007	-0.004	0.001	0.011	0.014	0.014
bias (%)	-0.150	-0.098	0.071	0.052	-0.071	0.091	-0.069	0.380
RMS (%)	2.300	2.737	2.952	2.757	2.405	1.463	1.455	1.481
Libya-1	band1	band2	band3	band4	band5	band6	band7	band8
fiso	0.190	0.193	0.209	0.222	0.290	0.473	0.503	0.584
fvol	0.288	0.252	0.208	0.208	0.211	0.177	0.131	0.144
fgeo	-0.017	-0.012	-0.007	-0.005	0.001	0.010	0.014	0.014
bias (%)	-0.331	-0.483	-0.356	-0.386	-0.398	-0.129	-0.264	0.067
RMS (%)	2.105	2.409	2.430	2.395	2.208	1.280	1.328	1.216
Libya-4	band1	band2	band3	band4	band5	band6	band7	band8
fiso	0.216	0.223	0.241	0.254	0.315	0.442	0.465	0.552
fvol	0.312	0.273	0.233	0.225	0.199	0.155	0.117	0.125
fgeo	-0.016	-0.011	-0.006	-0.003	0.004	0.011	0.014	0.014
bias (%)	-0.142	-0.317	-0.244	-0.254	-0.279	-0.145	-0.268	0.069
RMS (%)	1.422	1.509	1.655	1.651	1.689	1.176	1.241	1.111
Mauritania-1	band1	band2	band3	band4	band5	band6	band7	band8
fiso	0.192	0.192	0.203	0.213	0.269	0.439	0.467	0.544
fvol	0.266	0.208	0.154	0.150	0.153	0.154	0.127	0.149
fgeo	-0.019	-0.014	-0.008	-0.006	0.000	0.009	0.013	0.013
bias (%)	-0.066	-0.129	0.108	0.001	-0.167	-0.090	-0.268	0.151
RMS (%)	2.739	3.118	3.136	2.907	2.485	1.774	1.841	1.725
Mauritania-2	band1	band2	band3	band4	band5	band6	band7	band8
fiso	0.181	0.178	0.185	0.192	0.240	0.394	0.423	0.499
fvol	0.265	0.200	0.139	0.139	0.148	0.161	0.145	0.171
fgeo	-0.016	-0.012	-0.006	-0.004	0.002	0.008	0.012	0.011
bias (%)	-0.166	-0.144	-0.027	-0.135	-0.610	-0.847	-0.680	-0.171
RMS (%)	2.753	3.256	3.385	3.187	2.675	2.043	2.044	1.689

f_{iso}, f_{vol} and f_{geo} stand for the BRDF parameters, bias means the average of modeling error.

at each band for further analysis.

BRDF normalized time series

Again we use the example of Algeria-3 to present the detailed discussion of R^{TOA} time series and the corresponding linear trend in Fig. 6, while TABLE III presents the whole description of R^{TOA} time series over six PICSs. Since R^{TOA} (ρ^{TOA}/ρ^{BRDF}) and BRDF modeling error (ρ^{BRDF}-ρ^{TOA}) is negatively correlated, it is not surprising to find similar time series pattern between Fig. 6 and Fig. 4 (b), and the RMS of linear trend fitting residual is highly correlative to that of BRDF modeling errors because the slopes are close to 0 and intercepts are near 1. This RMS (indicating the drift limits of BRDF modeling error or R^{TOA}) could serve as a quantification of the stability of each site, and this stability is obviously spectrally dependent (~3% at SV bands and ~1.5% at red/NIR) caused by the reasons we mentioned above.

Then we focus on the linear trend analysis. The slope values in TABLE III of the fitted lines ranged from the order of 10^{-8} to 10^{-6}, corresponding to yearly change of 0.006% − 0.26%. Except for some cases at red/NIR bands (red colored in TABLE III), the *p* values of T-test are less than 0.05, indicating that the derived trends is mostly significant considering the < 0.3% stability of SeaWiFS over 13 years [16]. However, this slow change rate and the weakly significant *R* values (mostly less than 0.3) still represent a very stable long-term response (conforming to the definition of "pseudo-invariant").

The trend results of Algeria-3 also exhibit similar spectral characteristics. For SV bands, the slopes and *R* values are generally larger with intercepts more deviate to 1 (indicating the variant extent of R^{TOA} is more obvious) than at red/NIR bands. Except for Mauritania-2 (where linear variant rate appears more evident at channels 5 – 7 than at other bands, see blue colored records), the trending results generally show favorable stability at red/NIR bands (change per year within 0.15%), while that at SV channels are more uncertain (especially at Algeria-3). This confirms again the overall better stability at red/NIR bands because of less significant atmospheric impacts. The more significant trending results of red/NIR bands at Mauritania-2 could not be explained within the current dataset and needs further investigation, while

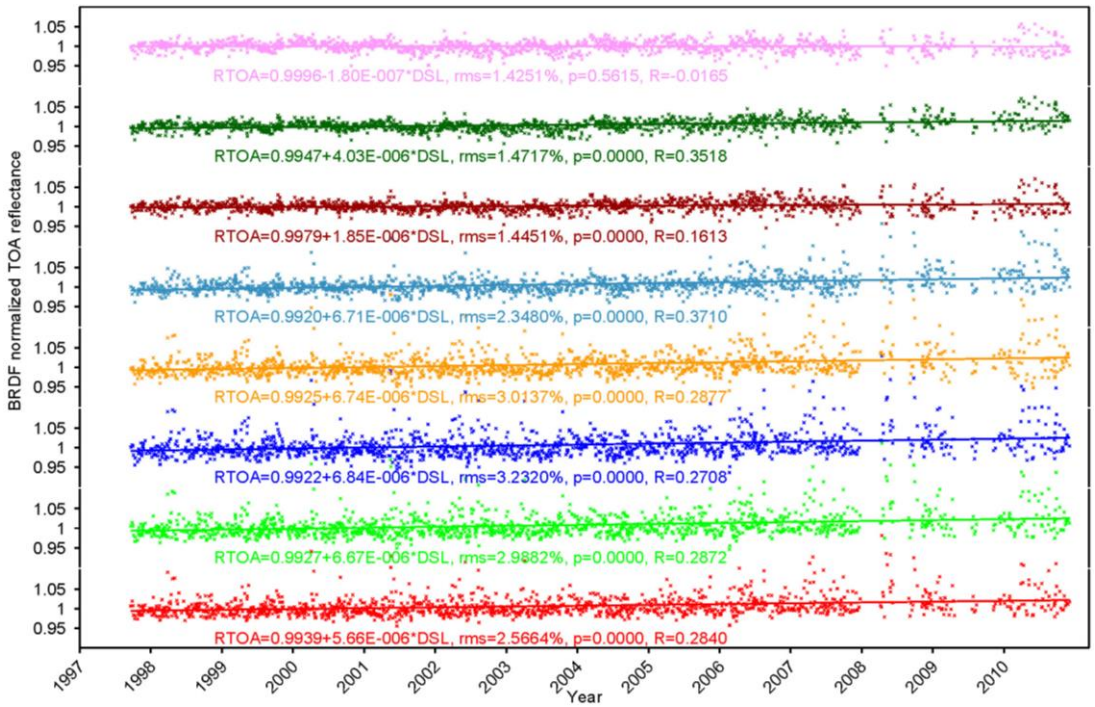

Fig. 6. Time series of BRDF normalized TOA reflectance over Algeria-3, with colored channel legend as in Fig. 4.

the relatively worse BRDF modeling performance at this site might be accounted for.

Although the derived time series of SeaWiFS data is of high stability as revealed above, the reliability of SeaWiFS data is expected to vary with time despite the rigorous post reprocessing. From the above discussion the orbit drift problem is apparently presented, and the data vacuum cases after 2008 also imply the data quality degradation. In addition, the more dispersion of error distribution in late operational years of SeaWiFS (2006 – 2010) compared to early mission data is also significant as seen from Fig. 4 (b). Therefore, we make a simple investigation of SeaWiFS data quality evolution based on independent BRDF fitting results of ρ^{TOA} over Algeria-3 during different periods, namely 1997 – 1998, 1999 – 2001, 2002 – 2004, 2005 – 2007, and 2008 – 2010. The fitting residuals (bias and RMS) are plotted in Fig. 7, which (for every band) are stable in 1997 – 2001 and exhibit a uniform increasing trend during the last three periods. Particularly, they present a sharp increase during 2008-2010 period, as expected from the effects of both drift and data vacuum problems. The biases of channel 1 – 4 in 2008 – 2010 are more than three times that in 1999 – 2001, and the corresponding RMSs also increase nearly two times. This temporal pattern could only be explained by more instrumental noise induced by

sensor aging after the design lifetime (five years) is passed. On the other hand, the red/NIR channels are again less

TABLE III

SUMMARY OF TREND ANALYSIS OVER SIX PICSS

p stands for the p value after t-test, *r* indicates the pearson correlation coefficient, and RMS is the root mean square of linear trend fitting residual.

Algeria-3	band1	band2	band3	band4	band5	band6	band7	band8
fiso	0.175	0.172	0.176	0.185	0.239	0.403	0.439	0.504
fvol	0.291	0.234	0.173	0.172	0.188	0.174	0.145	0.164
fgeo	-0.017	-0.012	-0.007	-0.004	0.000	0.010	0.013	0.014
bias (%)	-0.530	-0.601	-0.564	-0.590	-0.562	-0.158	-0.302	0.097
RMS (%)	2.413	2.785	2.998	2.799	2.218	1.427	1.448	1.430
Algeria-5	band1	band2	band3	band4	band5	band6	band7	band8
fiso	0.174	0.171	0.178	0.186	0.236	0.432	0.467	0.545
fvol	0.282	0.223	0.166	0.163	0.180	0.190	0.156	0.176
fgeo	-0.018	-0.013	-0.007	-0.004	0.001	0.011	0.014	0.014
bias (%)	-0.150	-0.098	0.071	0.052	-0.071	0.091	-0.069	0.380
RMS (%)	2.300	2.737	2.952	2.757	2.405	1.463	1.455	1.481
Libya-1	band1	band2	band3	band4	band5	band6	band7	band8
fiso	0.190	0.193	0.209	0.222	0.290	0.473	0.503	0.584
fvol	0.288	0.252	0.208	0.208	0.211	0.177	0.131	0.144
fgeo	-0.017	-0.012	-0.007	-0.005	0.001	0.010	0.014	0.014
bias (%)	-0.331	-0.483	-0.356	-0.386	-0.398	-0.129	-0.264	0.067
RMS (%)	2.105	2.409	2.430	2.395	2.208	1.280	1.328	1.216
Libya-4	band1	band2	band3	band4	band5	band6	band7	band8
fiso	0.216	0.223	0.241	0.254	0.315	0.442	0.465	0.552
fvol	0.312	0.273	0.233	0.225	0.199	0.155	0.117	0.125
fgeo	-0.016	-0.011	-0.006	-0.003	0.004	0.011	0.014	0.014
bias (%)	-0.142	-0.317	-0.244	-0.254	-0.279	-0.145	-0.268	0.069
RMS (%)	1.422	1.509	1.655	1.651	1.689	1.176	1.241	1.111
Mauritania-1	band1	band2	band3	band4	band5	band6	band7	band8
fiso	0.192	0.192	0.203	0.213	0.269	0.439	0.467	0.544
fvol	0.266	0.208	0.154	0.150	0.153	0.154	0.127	0.149
fgeo	-0.019	-0.014	-0.008	-0.006	0.000	0.009	0.013	0.013
bias (%)	-0.066	-0.129	0.108	0.001	-0.167	-0.090	-0.268	0.151
RMS (%)	2.739	3.118	3.136	2.907	2.485	1.774	1.841	1.725
Mauritania-2	band1	band2	band3	band4	band5	band6	band7	band8
fiso	0.181	0.178	0.185	0.192	0.240	0.394	0.423	0.499
fvol	0.265	0.200	0.139	0.139	0.148	0.161	0.145	0.171
fgeo	-0.016	-0.012	-0.006	-0.004	0.002	0.008	0.012	0.011
bias (%)	-0.166	-0.144	-0.027	-0.135	-0.610	-0.847	-0.680	-0.171
RMS (%)	2.753	3.256	3.385	3.187	2.675	2.043	2.044	1.689

influenced by this noise perturbation because of overall satisfactory fitting results in the whole mission, while the relative magnitude of residuals also expand significantly in 2008 – 2010 (~2 times for bias and ~1.5 times for RMS compared to that in 1999 – 2001). Therefore, we strongly suggest communities apply SeaWiFS data in early missions (e.g. 1997-2001) over these PICSs for calibration applications, as practiced by this study and others [5, 14].

Calibration applications

Among the examined PICSs, Libya-4 is the most preferable site from our analysis. From TABLE II and III, the fitting residuals at Libya-4 are within 1.7% at channels 1 – 5 and could be as small as ~1% at the other three bands, and the yearly percent change of R^{TOA} is within 0.15% at all bands. Therefore, a fixed BRDF model is sufficient to describe the long-term variation of ρ^{TOA} at Libya-4 based on its stability in more than one decade. This is the basis of inter-calibration works employing PICSs in recent studies [5, 6], where different BRDF models are employed to simulate the ρ^{TOA} for the referenced sensor (e.g. MODIS) at any given observing geometry ignoring the temporal variation for a given period, and then spectral adjustment (based on RT simulation or hyper-spectral measurements) could be applied to generate the

predicted ρ^{TOA} for the uncalibrated sensor (e.g. ETM or AVHRR). In this study, we derive the BRDF parameters for eight SeaWiFS bands at the six PICSs, and at least the results for channels 6 – 8 could be straightly adopted in similar applications. Because of more reliability of SeaWiFS data during early years as shown in Fig. 7 (e.g. 1997-2001), such calibration work should also consider applying early mission dataset to establish a SI traceable reference [5]. In terms of SV bands, the stability appears relatively less satisfactory, thus straightforwardly utilizing PICSs for calibration at such spectral regions is doubtable, and cares must be taken to reduce uncertainties from atmospheric effects (e.g. aerosols, ozone etc.). Nevertheless, the derived BRDF parameters for SV bands are still applicable in correcting a large part of directional effects (within ~3%) for sensor inter-comparisons, or absolute calibration if ρ^{TOA} could be obtained from other more reliable measurements rather than BRDF modeling. For example, during instrumented in situ calibration campaigns, the synchronism requirements of field and satellite observation could be loosen reasonably since the difference caused by different observing geometry could be reduced using this method, while confinements are still needed to guarantee similar atmospheric conditions for calibrating SV bands. Finally, the atmospheric effects would be more significant especially in large solar/viewing zenith angles because of prolonged scattering path, making the derived BRDF inadequate. Therefore in the above-mentioned calibration utilizations applying the derived BRDF results from our investigation for large zenith angles is not recommended without an extra evaluation of their performance in characterizing sensor received signals for such conditions.

CONCLUSION

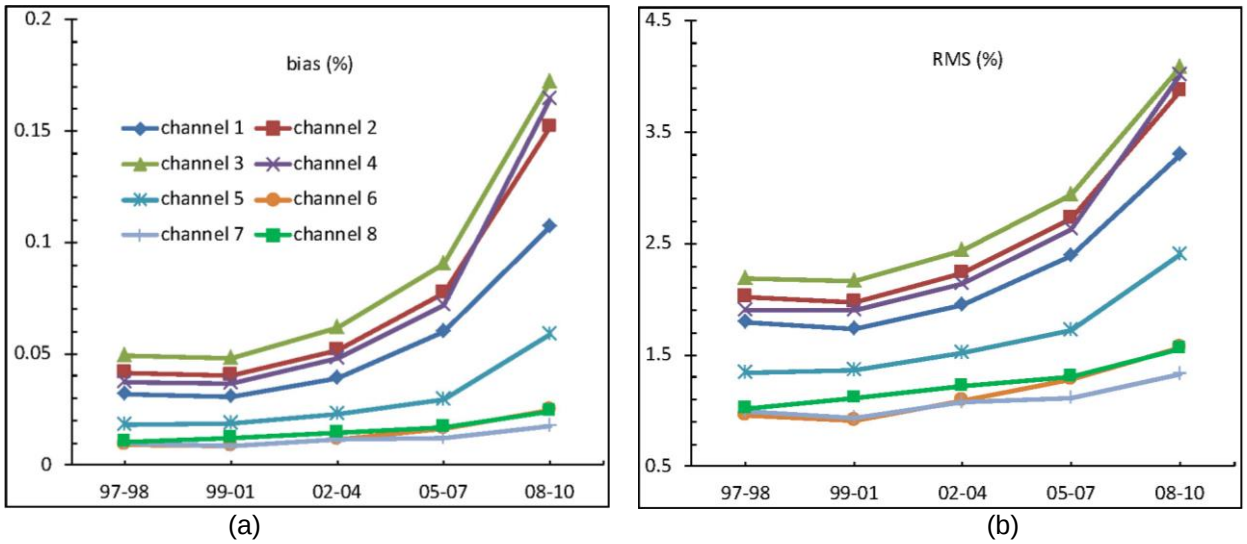

(a) (b)

Fig. 7. (a) Bias and (b) RMS of BRDF fitting residuals over Algeria-3 during five different periods.

Taking advantage of the high-quality SeaWiFS data, we quantify the long-term radiometric stability of spectral TOA reflectance over six CEOS endorsed PICSs. Considering the orbit tilt and drift issues of SeaWiFS, we resort to strict data screening and BRDF normalization to overcome the effects from abnormal observations and directional effects. In spite of the tilt and drift, the latest reprocessed SeaWiFS radiance data maintained lifetime stability, and from multi-spectral

data analysis of eight SeaWiFS bands complementary information is gained. From the BRDF fitting method we also discover that the data quality of SeaWiFS TOA radiance is less guaranteed in the late years, especially after 2008, suggesting extra data selection processing in particular applications. Finally, the derived results could be utilized directly or indirectly in various calibration applications, while the uncertainties induced by atmospheric dynamics (especially for SV channels) should be considered carefully.

4. Acknowledgement

This work would never be accomplished without the efforts made by the SeaWiFS Ocean Biology Processing Group for providing the SeaWiFS Level 1A data and the SeaDAS software. The authors are greatly thankful to the OBPG workers in establishing and maintaining the long-term data and processing tools used in this investigation.

References

[1] P. Teillet and G. Chander, "Terrestrial reference standard sites for postlaunch sensor calibration," *Canadian Journal of Remote Sensing*, vol. 36, pp. 437-450, 2010.

[2] G. Chander, T. J. Hewison, N. Fox, X. Wu, X. Xiong, and W. J. Blackwell, "Overview of Intercalibration of Satellite Instruments," *IEEE Transactions on Geoscience and Remote Sensing*, vol. 51, pp. 1056-1080, 2013.

[3] M. Dinguirard and P. N. Slater, "Calibration of space-multispectral imaging sensors: A review," *Remote Sensing of Environment*, vol. 68, pp. 194-205, 1999.

[4] G. Chander, X. Xiong, T. Choi, and A. Angal, "Monitoring on-orbit calibration stability of the Terra MODIS and Landsat 7 ETM+ sensors using pseudo-invariant test sites," *Remote Sensing of Environment*, vol. 114, pp. 925-939, 2010.

[5] A. Wu, X. Xiong, and A. Angal, "Derive a MODIS-Based Calibration for the AVHRR Reflective Solar Channels of the NOAA KLM Operational Satellites," *IEEE Transactions on Geoscience and Remote Sensing*, vol. 51 (3), pp. 1405-1413, 2013.

[6] D. Helder, K. J. Thome, N. Mishra, G. Chander, X. Xiong, A. Angal, *et al.*, "Absolute Radiometric Calibration of Landsat Using a Pseudo Invariant Calibration Site," *IEEE Transactions on Geoscience and Remote Sensing*, vol. 51, pp. 1360-1369, 2013.

[7] D. R. Potts, S. Mackin, J.-P. Muller, and N. Fox, "Sensor Intercalibration Over Dome C for the ESA GlobAlbedo Project," *IEEE Transactions on Geoscience and Remote Sensing*, vol. 51, pp. 1139-1146, 2013.

[8] R. A. Barnes, R. E. Eplee, F. S. Patt, H. H. Kieffer, T. C. Stone, G. Meister, *et al.*, "Comparison of SeaWiFS measurements of the Moon with the US Geological Survey lunar model," *Applied optics*, vol. 43, pp. 5838-5854, 2004.

[9] J.-Q. Sun, X. Xiong, W. L. Barnes, and B. Guenther, "MODIS reflective solar bands on-orbit lunar calibration," *IEEE Transactions on Geoscience and Remote Sensing*, vol. 45, pp. 2383-2393, 2007.

[10] X. Xiong and W. Barnes, "An overview of MODIS radiometric calibration and characterization," *Advances in Atmospheric Sciences*, vol. 23, pp. 69-79, 2006.

[11] C. Cao, E. Vermote, and X. Xiong, "Using AVHRR lunar observations for NDVI long-term climate change detection," *Journal of Geophysical Research*, vol. 114, doi:10.1029/2009JD012179, 2009.

[12] H. Cosnefroy, M. Leroy, and X. Briottet, "Selection and characterization of Saharan and Arabian desert sites for the calibration of optical satellite sensors," *Remote Sensing of Environment*, vol. 58, pp. 101-114, 1996.

[13] C. Cao, S. Uprety, J. Xiong, A. Wu, P. Jing, D. Smith, *et al.*, "Establishing the Antarctic Dome C community reference standard site towards consistent measurements from Earth observation satellites," *Canadian Journal of Remote Sensing*, vol. 36, pp. 498-513, 2010.

[14] A. Wu, A. Angal, X. Xiong, and C. Cao, "Using CEOS reference standard test sites to track the calibration stability of NOAA-19 AVHRR reflective solar channels," in *Proc. SPIE—Sensors, Systems, and Next-Generation Satellites XIV*, 2010, vol. 7826, p. 782 621.

[15] D. L. Helder, B. Basnet, and D. L. Morstad, "Optimized identification of worldwide radiometric pseudo-invariant calibration sites," *Canadian Journal of Remote Sensing*, vol. 36, pp. 527-539, 2010.

[16] R. E. Eplee Jr, G. Meister, F. S. Patt, B. A. Franz, and C. R. McClain, "Uncertainty assessment of the SeaWiFS on-orbit calibration," in *SPIE Optical Engineering+ Applications*, 2011, pp. 81530B-81530B-17.

[17] C. C. Molling, A. K. Heidinger, W. C. Straka, and X. Wu, "Calibrations for AVHRR channels 1 and 2: review and path towards consensus," *International Journal of Remote Sensing*, vol. 31, pp. 6519-6540, 2010.

[18] C. Schlundt, A. A. Kokhanovsky, W. von Hoyningen-Huene, T. Dinter, L. Istomina, and J. P. Burrows, "Synergetic cloud fraction determination for SCIAMACHY using MERIS," *Atmospheric Measurement Techniques*, vol. 4, pp. 319-337, 2011.

[19] L. Sun, X. Hu, M. Guo, and N. Xu, "Multisite Calibration Tracking for FY-3A MERSI Solar Bands," *IEEE Transactions on Geoscience and Remote Sensing*, vol. 50, pp. 4929-4942, 2012.

[20] R. Latifovic, D. Pouliot, and C. Dillabaugh, "Identification and correction of systematic error in NOAA AVHRR long-term satellite data record," *Remote Sensing of Environment*, vol. 127, pp. 84-97, 2012.

[21] A. K. Heidinger, W. C. Straka, C. C. Molling, J. T. Sullivan, and X. Wu, "Deriving an inter-sensor consistent calibration for the AVHRR solar reflectance data record," *International Journal of Remote Sensing*, vol. 31, pp. 6493-6517, 2010.

[22] S. Hooker and C. McClain, "The calibration and validation of SeaWiFS data," *Progress in Oceanography*, vol. 45, pp. 427-465, 2000.

[23] C. B. Schaaf, F. Gao, A. H. Strahler, W. Lucht, X. Li, T. Tsang, *et al.*, "First operational BRDF, albedo nadir reflectance products from MODIS," *Remote sensing of Environment*, vol. 83, pp. 135-148, 2002.

[24] N. C. Hsu, S.-C. Tsay, M. D. King, and J. R. Herman, "Aerosol properties over bright-reflecting source regions," *IEEE Transactions on Geoscience and Remote Sensing*, vol. 42, pp. 557-569, 2004.